Available online at www.sciencedirect.com
ScienceDirect
Journal of Catalysis 246 (2007) 127–135
JOURNAL OF CATALYSIS
www.elsevier.com/locate/jcat

# Enantioselectivity of immobilized Mn-salen complexes: A computational study

Kourosh Malek [a,*], Antonius P.J. Jansen [a], Can Li [b], Rutger A. van Santen [a]

[a] *Schuit Institute of Catalysis, ST/SKA, Eindhoven University of Technology, P.O. Box 513, 5600 MB, Eindhoven, The Netherlands*
[b] *State Key Laboratory of Catalysis, Dalian Institute of Chemical Physics, Chinese Academy of Sciences, Dalian, 116023, China*

Received 11 April 2006; revised 8 November 2006; accepted 21 November 2006

Available online 4 January 2007

**Abstract**

We use molecular dynamic simulations to investigate the origin of enantioselectivity of an anchored Mn-salen complex in MCM-41. This study provides new insight into the steric effects that relate to choices of substrate and linker and to the interplay with mesopore confinement. Avnir's continuous chirality measure method is adopted to quantify the chirality content of the Mn-salen complex. We show that the immobilized linker influences the enantioselectivity of the catalyst due to the increasing chirality content of the Mn-salen complex. Simulations with docked olefin ($\beta$-methyl styrene) suggest that *cis*- and *trans*-substrates have different level of asymmetric induction to the Mn-salen catalyst. A *trans*-substrate induces higher chirality to the immobilized Mn-salen complex than *cis*-olefin. We rationalize the importance of immobilization and show how it relates to the steric communication between the substrate and the Mn-salen complex. These results are important for the interpretation of the enantioselectivity of immobilized organometallic catalysts in nanoporous materials.


*Keywords:* Enantioselectivity; Immobilization; Heterogeneous catalysis; Mn-salen; Nanoporous materials; Chirality

## 1. Introduction

Immobilized $Mn^{III}$(salen) complexes on nanoporous materials have recently been proposed as a novel class of heterogeneous enantioselective catalyst for epoxidation of unfunctionalized olefins [1–6]. The porous hosted materials affect catalytic performance due to a cooperative interaction among the nanoporous solid, immobilizing linker, and Mn-salen complex [1,4,6]. Along with hydrothermal stability and excellent enantioselectivity, this attractive strategy has the inherent advantages of heterogeneity, such as easy separation and operation. Mesoporous materials are the most applicable supports for the immobilization of Mn-salen complexes [1,3]. $Mn^{III}$(salen) complexes have been successfully anchored in the mesopores of MCM-41 through the complexation of manganese by oxygen atoms of a linkage grafted on the surface of MCM-41 [1–4]. It has been shown that these heterogeneous catalysts give different excess enantioselectivity (ee) values for asymmetric epoxidation of *cis*-$\beta$-methyl styrene than their homogeneous counterparts [1,7,8]. The mesopore size and linkage length were found to be the most significant factors influencing the stereoselectivity of the immobilized Mn-salen catalysts [7]. The choice of *cis*- or *trans*- (*Z* or *E*) olefin as the substrate is another important issue worthy of further investigation [8]. Despite the numerous experimental and computational studies on various homogeneous Mn-salen-based catalysts, the exact mechanism of the Mn-salen complex reaction remains unclear [9–17]. Although the origin of the enantioselectivity of Mn-salen complexes has been extensively investigated by first-principle calculations [10–12], the mechanism of epoxidation of olefins by a heterogeneous immobilized Mn-salen catalyst cannot be trivially inferred from that occurring with homogeneous catalysts. The mechanism of enantioselective induction is not well known from a microscopic standpoint, and a detailed computational study on the immobilized Mn-salen/MCM-41 system has not been reported. There is lack of systematic theoretical and computational studies on the catalytic properties of the immobilized Mn-salen complexes as a function of substrate, nanoporosity, immobilizing linker, and enantioselectivity. An improved un-

* Corresponding author.
*E-mail address:* k.malek@tue.nl (K. Malek).

0021-9517/$ – see front matter 
doi:10.1016/j.jcat.2006.11.024

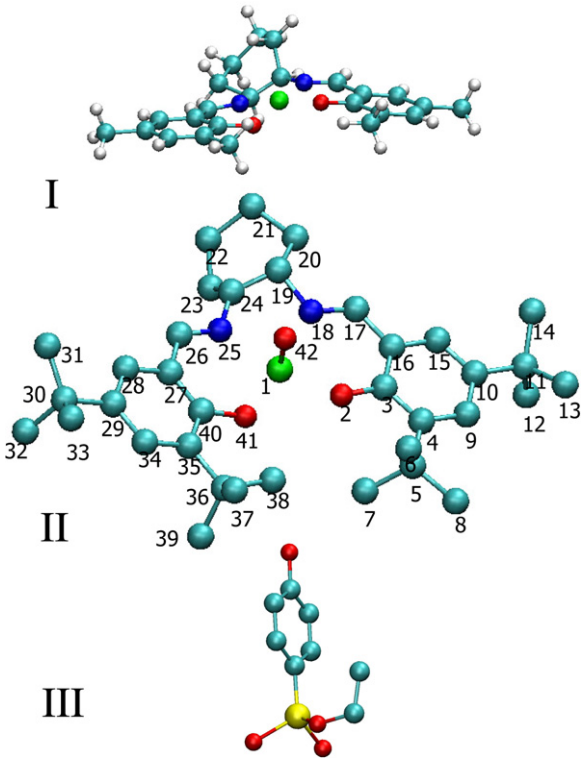


Scheme 1. The initial structure of Mn-salen complex (I), oxo-Mn-salen intermediate (II) and axial linker (III).

derstanding of how confinement and stereochemical effects of the nanopores and immobilizing agents influence the choice of enantioselective reaction path is important. In the present work, we used full-atom molecular dynamic simulations to investigate the steric inductions on the Mn-salen complex immobilized on the internal surface of a MCM-41 channel. We particularly wish to demonstrate the influence of the confined framework, substrate (*cis*- vs *trans*-) and immobilizing linker on the conformation of the immobilized Mn-salen complex. To translate this into practice, we use the continuous chirality measure (CCM) to quantitatively evaluate the distortion of Mn-salen complex. We then evaluate the chirality of the complex and compare it with that of a free complex in vacuo and that of a free complex within the MCM-41 mesopore. We perform independent simulations in the presence of a docked *cis*- and *trans*-$\beta$-methyl styrene as the substrate, for which we analyze the steric interactions by means of Mn-salen complex dynamics.

## 2. Methodology

### 2.1. Mn(salen), axial linkage and MCM-41 structures

The initial "step-like" structure of the Mn-salen complex was taken from the Cambridge database (ID:AFAXIO) from which structure I was made (Scheme 1). The oxo-$Mn^{V}$ intermediate II carries the activated oxygen that will be attached to the olefin double bond [9,15]. Mn-salen complexes have been successfully immobilized into MCM-41 nanopores, using a phenoxyl or phenyl sulfide group as the immobilizing linker [1–3]. In our simulations, salen complex II is used as the model catalyst, attaching to phenoxyl group as the immobilizing linker. The structure of axial linkage III, structure II, and olefins were later minimized in GAUSSIAN03 [18] using B3LYP functional [19] with a 6-31G* basis set [20], and the partial charges were simply taken from the Mulliken population analysis (Table 1). For all DFT calculations, a convergence criterion of $1.0 \times 10^{-6}$ au was adopted for changes in energy and density matrix elements. Local minima on the potential energy surface were characterized by real frequencies. Here intermediate II is considered the basic complex in all of the simulation setups, and reference is made to the atom numbering shown in Scheme 1. A generally accepted structure for MCM-41 materials consists of a hexagonal array of long, one-dimensional cylindrical pores in a range of 2.5–10 nm embedded in a matrix of amorphous silica [21]. Numerous models of MCM-41, with different approaches and degrees of surface heterogeneity and complexity, have been presented in the literature [21,22]. In

Table 1
Atomic data for Mn-salen complex II

| # | Atom | Type | Charge |
|---|---|---|---|
| 1 | O2 | om (esff) | −0.5 |
| 2 | MN42 | Mn036 (esff) | 0.5 |
| 3 | C3 | CB | 0.1 |
| 4 | C4 | CB | 0.1 |
| 5 | C5 | CB | 0.1 |
| 6 | C6 | CH3 | −0.1 |
| 7 | C7 | CH3 | −0.1 |
| 8 | C8 | CH3 | −0.1 |
| 9 | C9 | CR61 | −0.1 |
| 10 | C10 | CB | 0.1 |
| 11 | C11 | CB | 0.1 |
| 12 | C12 | CH3 | −0.1 |
| 13 | C13 | CH3 | −0.1 |
| 14 | C14 | CH3 | −0.1 |
| 15 | C15 | CR61 | −0.1 |
| 16 | C16 | CB | 0.1 |
| 17 | C17 | CR61 | −0.1 |
| 18 | N18 | nb (esff) | −0.5 |
| 19 | C19 | CH1 | 0.05 |
| 20 | C20 | CH2 | 0.05 |
| 21 | C21 | CH2 | 0.05 |
| 22 | C22 | CH2 | 0.05 |
| 23 | C23 | CH2 | 0.05 |
| 24 | C24 | CH1 | 0.05 |
| 25 | N25 | nb (esff) | −0.5 |
| 26 | C26 | CR61 | −0.1 |
| 27 | C27 | CB | 0.1 |
| 28 | C28 | CR61 | −0.1 |
| 29 | C29 | CB | 0.1 |
| 30 | C30 | CB | 0.1 |
| 31 | C31 | CH3 | −0.1 |
| 32 | C32 | CH3 | −0.1 |
| 33 | C33 | CH3 | −0.1 |
| 34 | C34 | CR61 | −0.1 |
| 35 | C35 | CB | 0.1 |
| 36 | C36 | CB | 0.1 |
| 37 | C37 | CH3 | −0.1 |
| 38 | C38 | CH3 | −0.1 |
| 39 | C39 | CH3 | −0.1 |
| 40 | C40 | CB | 0.1 |
| 41 | O41 | om (esff) | −0.5 |
| 42 | O42 | o′ (esff) | −0.5 |

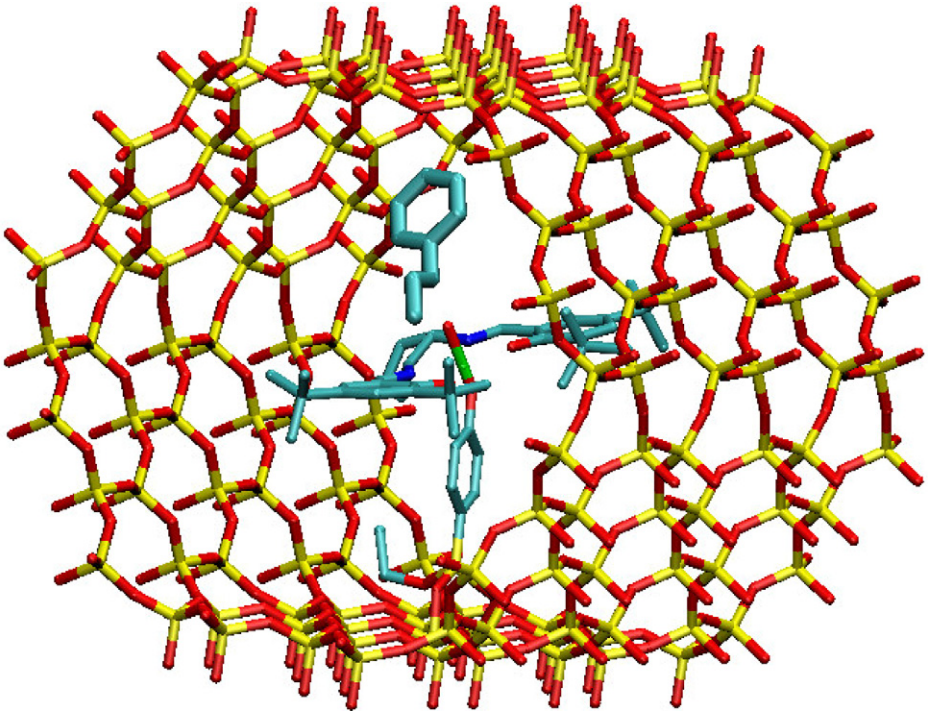

Fig. 1. An oxo-$Mn^{III}$(salen) complex anchored in a MCM-41 channel along with a docked *trans*-olefin [OACM(tr) system].

most of these models, the oxygen atoms are arranged in regular or stochastic arrays with layers of silicon atoms between each layer of oxygen atoms. In our MD simulations, MCM-41 channels are modeled based on straight, three-dimensional channels (Fig. 1). This modeling places the silicon and oxygen atoms in a simple geometrical arrangement and does not reproduce the real amorphous structure of MCM-41; however, it facilitates easy setup and fast simulation. Moreover, the framework can fluctuate according to the equation of motion. The structure is obtained by a pseudocell, $Si_6O_{12}$, consisting of hexagon arrangements of Si–O–Si units. Oxygen atoms saturate all silicon atoms at the pore surface. Oxygen atoms with fewer than two silicon atoms attached at the inlet, outlet, and outer surface are then saturated by hydrogen atoms. In our MCM-41 model, all hydroxyl groups are located at the outer surface. The pore length is 3.4 nm, and the pore diameter is 2.3 nm. Immobilization is performed by attaching the Si atom of the linker to oxygen atoms connected to two Si atoms on the wall ($Si_{Linker}$–O–$Si_{MCM}$).

### 2.2. Molecular dynamics (MD) calculations

All simulations were carried out using a fully atomistic model of Mn-salen complex, phenoxyl linker, and MCM-41 channel. Using MD simulations, we attempt to explain the enantioselectivity of an immobilized Mn-salen complex in MCM-41 in terms of the dynamics of the salen ligand. Due to the interactions with axial linkage and MCM-41, the Mn-salen complex may prefer a distorted conformation. We performed simulations using a modified version of the GROMOS96 force field [23,24] by adapting the nonbonding and bonding parameters of Mn and Si from the ESFF force field [25]. ESFF is an ab initio-derived force field, covering all atoms up to Rn in the periodic table. The parameterization in ESFF has been shown to be sufficient for organometallic compounds such as the salen complexes [25,26]. In our force field, interactions between atoms are divided into nonbonded interactions between any pair of atoms within a given cutoff radius and bonded interactions between atoms connected by chemical bonds. In nonbonded interactions (electrostatic and van der Waals), a partial charge and parameters for repulsion and attraction are assigned to each atom. The bonded interaction consists of bond, angle, and dihedral terms. The improper dihedrals represent the energy involved in changing the out-of-plane angles. The bond-stretching potential is expressed in terms of a Morse function, and bond-angle bending is given by simple harmonic potentials. The torsional rotation potential for the dihedral angle is a periodic function with a threefold barrier. The specific force field atom types and force parameters for the Mn-salen ligand are listed in Table 2. The default bond lengths and force constants are later converted to Morse parameters. The partial charges and interaction parameters for all other species (methyl styrene and phenoxyl linker) were taken from GROMOS96 database [23,24]. A typical effective potential is of the form

$$
\begin{aligned}
V = {} & \sum_{\text{bond}} D_{\text{b}i}\left[1-\exp\left(-\alpha_i\left(r-r_i^0\right)\right)\right]^2 \\
& + \sum_{\text{angles}} \frac{K_{\text{a}i}}{\sin^2\theta_i^0}\left[\cos\theta-\cos\theta_i^0\right]^2 \\
& + \sum_{\text{dihedrals}} k^{\Phi}\left(1+\cos\left(n\left(\Phi-\Phi^0\right)\right)\right) \\
& + \sum_{i<j}\frac{A_{ij}}{r_{ij}^{12}}-\frac{B_{ij}}{r_{ij}^{6}}+\sum_{i<j}\frac{\operatorname{erfc}(\beta r_{ij})}{4\pi\epsilon_0 r_{ij}}q_i q_j, \qquad (1)
\end{aligned}
$$

Table 2
Equilibrium bond (a), angle (b) and dihedral (c) and their corresponding energy barriers for Mn-salen complex II. Atom numbers are similar to those in Table 1

(a)

| $i$ | $j$ | $r_0$ (nm) | kJ/(mol nm$^2$) | $i$ | $j$ | $r_0$ (nm) | kJ/(mol nm$^2$) |
|---|---|---|---|---|---|---|---|
| 1 | 3 | 0.136 | 313800 | 19 | 24 | 0.142 | 418400 |
| 1 | 2 | 0.189 | 376560 | 20 | 21 | 0.154 | 418400 |
| 2 | 42 | 0.17 | 376560 | 21 | 22 | 0.154 | 418400 |
| 2 | 41 | 0.187 | 376560 | 22 | 23 | 0.154 | 376560 |
| 2 | 18 | 0.19 | 376560 | 23 | 24 | 0.154 | 313800 |
| 2 | 25 | 0.19 | 376560 | 24 | 25 | 0.132 | 376560 |
| 3 | 4 | 0.139 | 418400 | 25 | 26 | 0.128 | 376560 |
| 3 | 16 | 0.139 | 418400 | 26 | 27 | 0.146 | 334720 |
| 4 | 5 | 0.154 | 418400 | 27 | 28 | 0.139 | 376560 |
| 4 | 9 | 0.139 | 418400 | 27 | 40 | 0.139 | 418400 |
| 5 | 6 | 0.154 | 418400 | 28 | 29 | 0.139 | 376560 |
| 5 | 7 | 0.154 | 418400 | 29 | 30 | 0.154 | 418400 |
| 5 | 8 | 0.154 | 418400 | 29 | 34 | 0.139 | 418400 |
| 9 | 10 | 0.139 | 418400 | 30 | 31 | 0.154 | 418400 |
| 10 | 11 | 0.154 | 376560 | 30 | 32 | 0.154 | 418400 |
| 10 | 15 | 0.139 | 376560 | 30 | 33 | 0.154 | 418400 |
| 11 | 12 | 0.153 | 334720 | 34 | 35 | 0.139 | 418400 |
| 11 | 13 | 0.154 | 376560 | 35 | 36 | 0.154 | 418400 |
| 11 | 14 | 0.154 | 418400 | 35 | 40 | 0.138 | 376560 |
| 15 | 16 | 0.139 | 376560 | 36 | 37 | 0.154 | 313800 |
| 16 | 17 | 0.139 | 418400 | 36 | 38 | 0.154 | 418400 |
| 17 | 18 | 0.129 | 418400 | 36 | 39 | 0.154 | 376560 |
| 18 | 19 | 0.146 | 418400 | 40 | 41 | 0.136 | 313800 |
| 19 | 20 | 0.154 | 418400 | | | | |

(b)

| $i$ | $j$ | $k$ | $\theta_0$ (deg) | kJ/(mol deg$^2$) | $i$ | $j$ | $k$ | $\theta_0$ (deg) | kJ/(mol deg$^2$) |
|---|---|---|---|---|---|---|---|---|---|
| 1 | 3 | 4 | 116.5 | 397.5 | 21 | 22 | 23 | 109.5 | 460.2 |
| 1 | 3 | 16 | 123 | 418.4 | 22 | 23 | 24 | 120 | 418.4 |
| 1 | 2 | 42 | 89 | 418.4 | 19 | 24 | 23 | 120 | 418.4 |
| 4 | 3 | 16 | 120 | 418.4 | 19 | 24 | 25 | 109.5 | 460.2 |
| 3 | 4 | 5 | 120 | 418.4 | 23 | 24 | 25 | 109.5 | 460.2 |
| 3 | 4 | 9 | 120 | 418.4 | 24 | 25 | 26 | 109.5 | 460.2 |
| 5 | 4 | 9 | 120 | 418.4 | 25 | 26 | 27 | 109.5 | 460.2 |
| 4 | 5 | 6 | 120 | 418.4 | 26 | 27 | 28 | 109.5 | 460.2 |
| 4 | 5 | 7 | 120 | 418.4 | 26 | 27 | 40 | 109.5 | 460.2 |
| 4 | 5 | 8 | 120 | 418.4 | 28 | 27 | 40 | 120 | 418.4 |
| 6 | 5 | 7 | 120 | 418.4 | 27 | 28 | 29 | 120 | 418.4 |
| 6 | 5 | 8 | 120 | 418.4 | 28 | 29 | 30 | 120 | 418.4 |
| 7 | 5 | 8 | 120 | 418.4 | 28 | 29 | 34 | 120 | 418.4 |
| 4 | 9 | 10 | 120 | 418.4 | 30 | 29 | 34 | 120 | 418.4 |
| 9 | 10 | 11 | 109.5 | 460.2 | 29 | 30 | 31 | 120 | 418.4 |
| 9 | 10 | 15 | 109.5 | 460.2 | 29 | 30 | 32 | 120 | 418.4 |
| 11 | 10 | 15 | 109.5 | 460.2 | 29 | 30 | 33 | 120 | 418.4 |
| 10 | 11 | 12 | 109.5 | 460.2 | 31 | 30 | 32 | 120 | 418.4 |
| 10 | 11 | 13 | 109.5 | 460.2 | 31 | 30 | 33 | 120 | 418.4 |
| 10 | 11 | 14 | 109.5 | 460.2 | 32 | 30 | 33 | 120 | 418.4 |
| 12 | 11 | 13 | 120 | 418.4 | 29 | 34 | 35 | 120 | 418.4 |
| 12 | 11 | 14 | 120 | 418.4 | 34 | 35 | 36 | 109.5 | 397.5 |
| 13 | 11 | 14 | 120 | 418.4 | 34 | 35 | 40 | 109.5 | 460.2 |
| 10 | 15 | 16 | 120 | 418.4 | 36 | 35 | 40 | 109.5 | 460.2 |
| 3 | 16 | 15 | 120 | 418.4 | 35 | 36 | 37 | 120 | 418.4 |
| 3 | 16 | 17 | 120 | 418.4 | 35 | 36 | 38 | 120 | 418.4 |
| 15 | 16 | 17 | 120 | 418.4 | 35 | 36 | 39 | 109.5 | 460.2 |
| 16 | 17 | 18 | 120 | 418.4 | 37 | 36 | 38 | 109.5 | 460.2 |
| 17 | 18 | 19 | 120 | 418.4 | 37 | 36 | 39 | 109.5 | 460.2 |
| 18 | 19 | 20 | 120 | 418.4 | 38 | 36 | 39 | 109.5 | 460.2 |
| 18 | 19 | 24 | 120 | 418.4 | 27 | 40 | 35 | 109.5 | 460.2 |
| 20 | 19 | 24 | 120 | 418.4 | 27 | 40 | 41 | 109.5 | 460.2 |
| 19 | 20 | 21 | 109.5 | 397.5 | 35 | 40 | 41 | 120 | 418.4 |
| 20 | 21 | 22 | 109.5 | 460.2 | 41 | 2 | 42 | 89 | 418.4 |

(*continued in the next column*)

Table 2 (*continued*)

(c)

| $i$ | $j$ | $k$ | $l$ | $\Phi$ (deg) | $K_\Phi$ kJ/(mol deg) |
|---|---|---|---|---|---|
| 3 | 8 | 4 | 1 | 0 | 1673.6 |
| 8 | 3 | 9 | 7 | 0 | 1673.6 |
| 15 | 20 | 16 | 14 | 0 | 1673.6 |
| 20 | 15 | 19 | 21 | 0 | 1673.6 |
| 15 | 16 | 17 | 18 | 0 | 1673.6 |
| 16 | 17 | 18 | 19 | 0 | 1673.6 |
| 17 | 18 | 19 | 20 | 0 | 1673.6 |
| 18 | 19 | 20 | 15 | 0 | 1673.6 |
| 19 | 20 | 15 | 16 | 0 | 1673.6 |
| 20 | 15 | 16 | 17 | 0 | 1673.6 |
| 3 | 4 | 5 | 6 | 0 | 1673.6 |
| 4 | 5 | 6 | 7 | 0 | 1673.6 |
| 5 | 6 | 7 | 8 | 0 | 1673.6 |
| 6 | 7 | 8 | 3 | 0 | 1673.6 |
| 7 | 8 | 3 | 4 | 0 | 1673.6 |
| 8 | 3 | 4 | 5 | 0 | 1673.6 |
| 8 | 3 | 1 | 2 | 180 | 7.1 |
| 3 | 8 | 9 | 10 | 180 | 41.8 |
| 8 | 9 | 10 | 11 | 180 | 33.5 |
| 12 | 11 | 10 | 9 | 180 | 0.4 |
| 13 | 12 | 11 | 10 | 0 | 5.9 |
| 11 | 12 | 13 | 14 | 180 | 0.4 |
| 12 | 13 | 14 | 15 | 180 | 33.5 |
| 20 | 15 | 14 | 13 | 180 | 41.8 |
| 15 | 20 | 21 | 22 | 180 | 7.1 |

where $r$ is the distance between atoms $i$ and $j$ (or united atoms when $CH_n$ groups are treated as one atom); $q_i$ is the partial charge on atom $i$; $\beta$ is a parameter that determines the relative weight of space sum; erfc is the complementary error function; $A_{ij}$ and $B_{ij}$ are Lennard-Jones parameters; $D_{bi}$, $K_{ai}$, and $k^\Phi$ are force constants for bonds, angles, and dihedrals; $n$ is the dihedral multiplicity; and $r_i^0$, $\theta_i^0$, $\Phi^0$ are equilibrium values for the bond lengths, angles, and dihedrals, respectively. $\alpha_i$ characterizes the anharmonicity of the bond. The most important assumption is that only pair interactions are taken into account; nonbonded interactions between three or more atoms are neglected. Moreover, atoms are represented as point charges, and thus electronic polarizability is neglected. The Si–O bond stretching potential and O–Si–O bond angle bending are given by simple harmonic potentials $V(R) = k_b(r_{Si-O} - r_{eq})/2$ and $V(\theta) = k_\theta(\theta - \theta_{eq})/2$, respectively, where $k_b = 2.5 \times 10^5$ kJ/(mol nm$^2$) and $k_\theta = 0.17605$ kJ/(mol deg$^2$). The torsional rotation potential for the Si–O–Si–O dihedral angle is a periodic function with a threefold barrier, $V(\Phi) = k^\Phi(1 + \cos(3f))/2$, where $k^\Phi = -2.9289$ kJ/mol [27]. The electrostatic interactions require special care. Because we are interested only in local interactions at isolated MCM-41/linker/oxo-Mn-salen/olefin interface, we imposed no periodic boundary conditions along the pore. Accordingly, no correction for the long-range electrostatic interactions is needed. Nevertheless, we imposed a continuum dielectric medium ($\epsilon = 20$) around the Mn-salen complex. The use of Ewald summation is especially correct when an infinite dielectric is assumed in the medium surrounding the interacting molecules [28]. Although no artefacts are associated with the truncation of electrostatic forces, we calculated the electrostatic interactions in our simulations using the Particle-Mesh Ewald (PME) method [28]

with a grid spacing of 0.12 nm and fourth-order interpolation. PME is a method for improving the performance of the reciprocal sum by applying a Fourier transformation on the grid. An inverse transformation and interpolation factors provide the potential and forces on each atom. When Ewald summation is used for long-range interactions, the short-range columbic potential must be modified. The last term in Eq. (1) shows the short-range electrostatic potential used in our simulations. The complication can be removed simply by expanding the potential energy cutoff to the dimension of the MCM-41 channel. In our simulation, we used a cutoff of 1.4 nm to ensure compatibility to that in the original force field. The force field was parameterized according to the electrostatic charges and Lennard-Jones parameters for the MCM-41, Mn-salen complex, and linkage. The atomic fluctuations were monitored by calculating the root mean squared deviations (RMSDs) between the X-ray structure and the time-averaged structure from MD calculations ($RMSD_{bond}$: 0.021 Å; $RMSD_{angle}$: 1.855°; $RMSD_{dihedral}$: 4.895°; $RMSD_{atom\text{-}position}$: 0.355 Å). During the simulation, the potential energy and the total energy were monitored to check whether the system is in equilibrium. Moreover, the profile of the RMSD of the atoms from the initial configuration was used to determine the equilibrium and stability of the system. MD simulations were performed in a canonical (NVT) ensemble at 273 K. For the simulations in the presence of a docked olefin, a harmonic position restraint (1000 kJ/(mol nm$^2$)) was applied on $\alpha$ and $\beta$ carbon atoms of the olefins. This position fixes the distance between C-$\alpha$ and oxo-oxygen at 0.28 nm, which corresponds to the equilibrium distance between C-$\alpha$ and oxygen during adsorption of olefin on Mn-salen [11]. A cutoff of 1.0 nm was used for van der Waals interactions, comparable to what was assumed originally in the force field. The integration time step was 2 fs. After the systems were equilibrated for 200 ps using harmonic position restraints (1000 kJ/(mol nm$^2$)), production runs were performed for another 5 ns, the last 4.5 of which was used for the analysis. The stable LINCS algorithm was used to constrain bond lengths and angles [23]. The temperature was controlled by the Berendsen algorithm, which mimics a weak coupling to an external heat bath with given temperature $T_0$ [24]. The effect of this weakly coupling algorithm is that a deviation of the system temperature from $T_0$ is slowly corrected according to

$$\frac{dT}{dt} = \frac{T_0 - T}{\tau_T}, \tag{2}$$

which means that a temperature deviation decays exponentially with a time constant $\tau_T$. In our simulations, the weak coupling algorithm was applied separately for the MCM-41 channel, linkage, and complex with a time constant of 0.1 ps at 273 K. During the production run, structures were saved every 500 steps (1 ps) and used for the analysis. In the present simulations, the –OH terminus was treated as a united atom, similar to CH, $CH_2$, and CH– aromatic. Simulations were done with the GROMACS package [29,30] (http://www.gromacs.org). Visualization was done using the VMD v1.8.1 [31] commercial package.

### 2.3. Continuous chirality measure (CCM)

A chiral center is usually recognized by a condition that no pair of groups attached to the atom in the center (e.g., carbon) is identical. Chirality is conventionally defined in tetravalent configurations and never for planar structures [32]. The degree of chirality or the disturbance of achirality also depends on the size and chemical nature of the groups attached to a chiral center. If a large group is used as a substituent in the chiral center, then the chirality of the molecule is not so pronounced [33]. In some cases, a pair of identical groups still produces chirality [32]. To explain these observations, a quantitative description of "chirality" is needed. Numerous approaches to quantifying chirality of an object [32–39] have been proposed. The Avnir CCM is one of the best models and has proven successful in many cases [33]. A continuous symmetry scale is able to express quantitatively how far a given distorted structure is from ideal symmetry [38]. We use the CCM method to compute the chirality content of the optimized geometries of the salen complex. The optimized geometry of the Mn-salen complex of different steps along the reaction pathways is used as input for the calculation of CCM. The measure is based on the minimal distance that the atoms of the molecule need to undergo to attain a desired symmetry, namely achirality. The structure of desired symmetry is not a priori and is obtained by optimization techniques for each configuration. The latter is the most time-consuming step in evaluating the chirality content of an object by the CCM approach [33–36]. $G$ is assumed to be the nearest achiral symmetry group to structure $Q$, composed of $N$ vertices (atoms) whose $3N$ Cartesian coordinates $q_k$ are arranged in $N$ vectors $\vec{q}_i$. The Cartesian coordinates of $G$-symmetry object, $p_k$, are contained in $N$ vectors $\vec{p}_i$. The chirality measure ($S$) of $Q$ with respect to $G$ is defined as

$$S_Q(G) = \frac{100}{ND^2} \sum_{i=1}^{N} |\vec{q}_i - \vec{p}_i|^2, \tag{3}$$

where $D$ is a normalization factor that makes CCM size-invariant. In analogy to a recent work by Handgraaf et al. [40], we take a slightly different approach to calculating the chirality of the complexes. Here we consider the mirror images of an enantiomeric pair. The minimum distance between the enantiomers is calculated by superimposing the random orientation of the enantiomers on each other. After superimposing two enantiomers by translation to the coordinates of the image to the Mn center, the image enantiomer is randomly rotated (by generating random angles using a spherical coordinate centered at Mn), until the minimum value of CCM is attained. Thus, the numerical optimization procedure is less complicated (although not necessarily less expensive) than the approach of finding a desired closest symmetry [Eq. (3)].

## 3. Results and discussion

The triplet and quintet spin states of the oxo-$Mn^V$-salen complex are of lower energy relative to the singlet state [15]. Puckered and step-like distortions exist for triplet and quintet

Table 3
Relative energies (kJ/mol) of spin states for truncated oxo-Mn-salen complex vs axial linkage

| Method | Spin state | Mn-salen-Cl | Mn-salen-phenoxyl |
|---|---|---|---|
| B3LYP | Singlet | 10 | 50 |
| B3LYP | Triplet | 0 | 0 |
| B3LYP | Quintet | 2 | 10 |

states, compared with the relatively flat, less chiral single-state geometry [34]. It also has been shown that no axial binding occurs in the singlet state [15]. The multiplicity at the ground state determines the initial configuration of the Mn-salen complex that we must take into account in our simulations. To investigate the possible configurations of the complex as a function of electronic multiplicity and axial linker, we performed a series of calculations based on density functional theory (DFT) with the B3LYP hybrid functional [19] in combination with 6-31G* [20] basis sets. We compared the optimized structure of truncated intermediate oxo-Mn-salen II [41] with Cl at the trans position to that in which this position is occupied by phenoxyl linker. Table 3 shows the effect of the linker on the relative energies of the different spin states, calculated by the Mn triple-$\xi$ basis/B3LYP/6-31G*. In the presence of Cl, the triplet state is the ground state, as reported previously [13,14]. Some studies have shown that the triplet state is almost isoenergetic with the single state [10]. Similarly, when the phenoxyl group is introduced, a triplet state becomes the most stable state. A step-like structure is taken as the starting configuration for the Mn-salen complex in our MD simulations, as was predicted by the DFT calculations. In conclusion, we assume that epoxidation reaction for both homogeneous catalysts (i.e., where Cl is the axial ligand) and heterogeneous catalysts (i.e., where phenoxyl group is the axial ligand) occurs on a triplet surface. Nevertheless, the reader should refer to previously published detailed accounts of spin-crossing along the reaction pathway [7,41,42]. Calculations suggest that the triplet state has the lowest energy and that a metallocyclic intermediate likely is not involved in the reaction, whereas the presence of a radical intermediate is evident [41]. It appears that the choice of calculation method (DFT vs HF), the basis set for geometry optimization (hybrid B3LYP vs pure BP86), as well as the choice of model system for salen ligand (truncated vs full ligand) cause many of the contradictions reported in the literature [41–43]. To avoid all such discrepancies, we limited ourselves to a widely accepted reaction mechanism on a triplet surface (Scheme 2). The conformational changes in the complex due to the interactions with the channel wall or interactions with the axial linkage are studied by different simulation setups; free complex in vacuo (FCV), free complex attached to linkage III in vacuo (FCL), free complex inside a MCM-41 channel (FCM), and an anchored complex inside a MCM-41 channel (ACM). Simulations also have been performed on the ACM system in the presence of *cis*- and *trans*-methyl styrene as the substrate, namely OACM(cis) and OACM(tr), respectively. Due to the interactions with the axial linkage and MCM-41, the Mn-salen complex may prefer a distorted conformation different from that for a homogeneous catalyst. Two main approach trajectories (side-

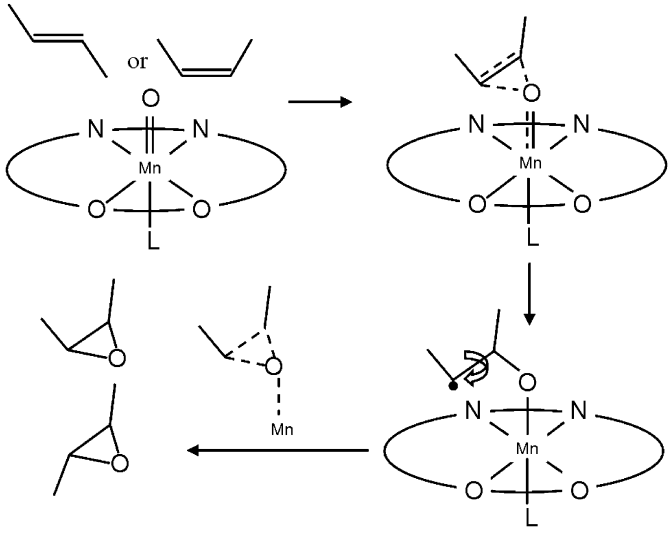


Scheme 2. General mechanism scheme for asymmetric epoxidation of olefins using Mn-salen complexes; L = axial linker.

on vs top-on) have been proposed to explain the degree and type of enantioselective communications between olefin and Mn-salen catalyst [44]. According to the side-on mechanism [9,13], the swinging and twisting motions of the phenyl groups and the 3,3′- and 5,5′-*tert*-butyls, together with the swinging of the cyclohexyl substituent, are the most important distortion features of the Mn-salen complex. Different types of dihedral angles (e.g., between atoms C40, C27, C26, and N25; between atoms C3, C16, C17, and N18; and those with a Mn=O bond) can characterize these conformational changes. It has been suggested that the steric constraints of the framework favor a certain conformation of the Mn-salen complex, so that this conformation is stable at room temperature [26]. The swinging of the cyclohexyl, as well as the twisting motion of the phenyl groups and their substituents, play important roles when the olefin approaches the oxo group (Mn=O) from the oxygen side. It is also important to note that the degree of distortion also depends on the initial orientation of the complex in the channel. Throughout our simulations, the equatorial *tert*-butyl ligands aligned along the channel axis. A perpendicular position in respect to the channel axis is unlikely, because this requires significant folding of the Mn-salen complex in the confined MCM-41 channel. Although several studies based on the most probable (dihedral) angles have provided insight into a preferable distorted conformation [10,26], a comprehensive description of the origin of the enantioselectivity has not been given. Following the recent pioneering works by Avnir [33–38] and others [32,39], it is now possible to compute the chirality of Mn-salen complexes as a function of twisting and swinging measures. An interesting correlation between the enantiomeric separation efficiency and the degree of chirality of the metal-complex catalyst has been established [33]. We adopt Avnir's CCM method [37,38,40] to quantify the chirality content of the optimized geometries of the Mn-salen complex. Such an analysis in terms of CCM rather than the pure geometry (i.e., angle analysis) can provide a more accurate assessment of the origin of enantioselectivity [33,40]. Assuming a side-on mechanism for the enantioselective epox-

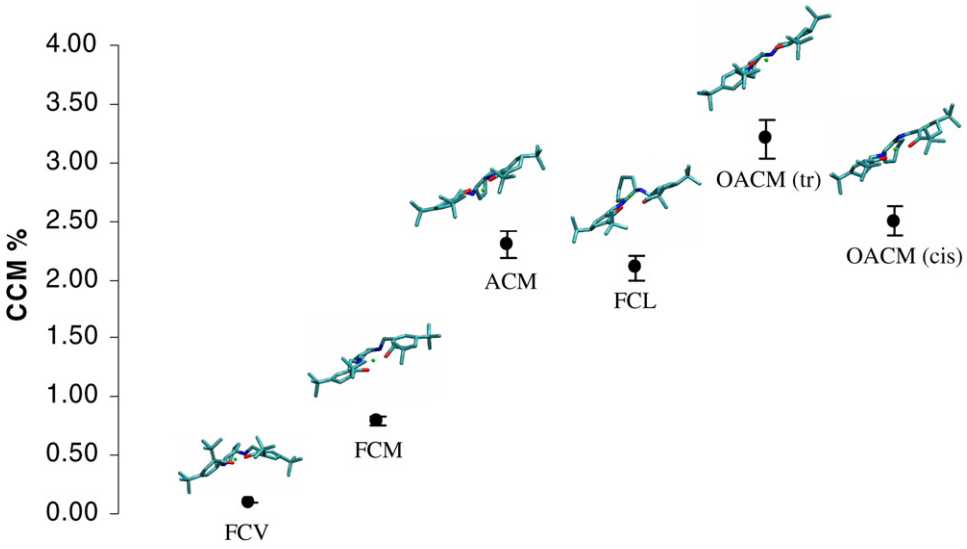


Fig. 2. CCM of Mn-salen in systems free complex in vacuo (FCV), free complex attached to linkage III in vacuo (FCL), free complex inside a MCM-41 channel (FCM), and an anchored complex inside MCM-41 channel (ACM). The configurations of the catalyst are averaged over all MD frames for each simulation set-up.

idation of methyl-styrene by Mn-salen/MCM-41 (Scheme 2), we show how chirality of the Mn-salen complex can be used as a reaction coordinate. Fig. 2 shows the CCM of Mn-salen complexes in systems FCV, FCM, ACM, FCL, OACM(cis), and OACM(tr). This profile provides the enantioselectivity induced by the axial linkage and MCM-41 channel in terms of chirality measure of the Mn-salen complex. For each system, the optimized structure of the complex at each time frame, 100 ps, is calculated by MD simulations and is used as the input for calculating the chirality content of the complex. The CCM is then averaged over all 45 configurations during 4.5 ns dynamics. The structures shown in Fig. 2 are averaged over all 45 configurations. The chirality increases for the immobilized catalyst; moreover, the presence of the olefin increases the chirality content of the complex. The CCM value for FCV (homogeneous complex) represents a cup-like structure close to C2 symmetry with a low chirality [34]. Deviations from cup-like geometry are seen in FCM and ACM. Significantly, in ACM and FCM, the motion of the phenyl groups shields one side of the complex more than the other, leading to step-like configurations with varying degrees of phenyl distortion (i.e., confinement effect). The CCM for FCL and ACM are close, meaning that the axial linkage plays a major role in the complex dynamics compared with the minor role of the MCM-41 channel. This may not be true for smaller channel sizes than those that we studied, when the complex is confined more to the inside of the channel. Our first important finding is that the staggered gauche conformation (di-imine bridge) formed in FCV slowly converts to the eclipsed gauche conformation in ACM. The latter corresponds to a boat-to-chair conformation transition in the cyclohexyl linkage. There is an obvious deviation from the configuration of the homogeneous complex. The deviation is such that the front side of the complex becomes more blocked by the bulky groups and thus may hinder the approach of the olefins from this side more so than from the other side. In contrast to FCV and FCM, in ACM a specific path for the approaching olefin is blocked. FCM and ACM have a different conformation than FCV, indicating that the complex inside MCM-41 is limited to structures with gauche conformation. The analysis shows that in certain conformations, 3,3′-*tert*-butyl substituents shield the olefin attack. The effect of cyclohexyl motion and 5,5′-substituents is small compared to that of phenyl movements. The second significant finding is that the CCM for a docked *trans*-olefin is higher than that for a *cis*-olefin. This is in contrast to the general assumption that *trans*-olefin provides a lower yield and ee than the *cis*-olefin for the immobilized system as well [9]. This is usually the case for a homogeneous catalyst. This controversy can be explained by a "lock-and-key" mechanism. A *trans*-olefin is less likely than a free Mn-salen complex to approach a complex with a so-called "cup-like" configuration. For an anchored Mn-salen, the step-like character is more significant. Whereas a *trans*-olefin is not a suitable substrate in a homogeneous Mn-salen catalyst (FCV, cup-like with low CCM), it can be asymmetrically catalyzed by an anchored complex on MCM-41 [OACM(tr), step-like, high CCM]. A *trans*-substrate indicates a preferred interaction with Mn-salen ligand when the complex is immobilized by a neutral donor ligand, such as phenoxyl group. On the other hand, a *cis*-olefin overcomes the same steric hindrances when it approaches the oxo-oxygen in step-like or in cup-like configurations. Therefore, in principle, *cis*-olefin can be a favorable substrate for both homogeneous and heterogeneous applications. We have also performed MD simulations at different points along the proposed side-on reaction mechanism. Fig. 3a illustrates the representative optimized structures of the Mn-salen complex along the reaction pathway. (The MCM-41 atoms were removed for clarity.) The structures were averaged and obtained as explained in Fig. 2. The structures contain the isolated oxo-Mn-salen (I), the anchored complex (II), docked olefin and encounter-complex of catalyst and substrate (III), reacting intermediate complexes of catalyst and substrate (IV), reaction intermediate state (V), complex of reacted catalyst and product (VI), deoxygenated anchored cat-

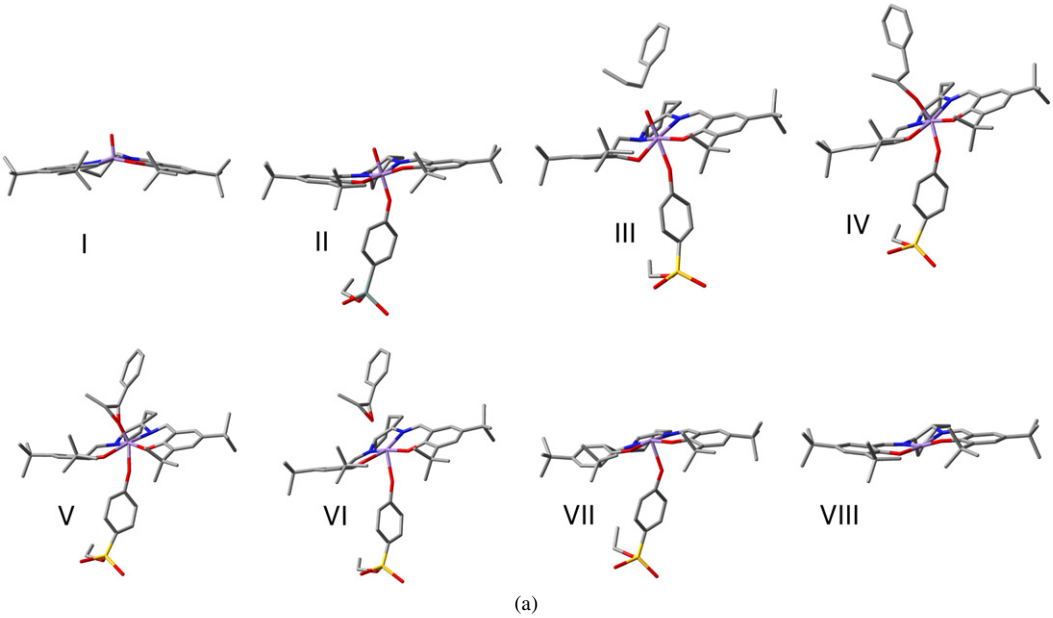


(a)

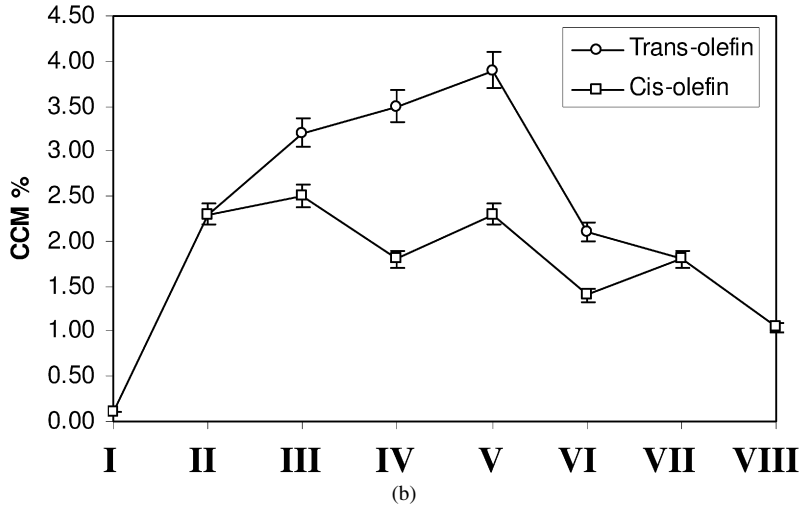


(b)

Fig. 3. (a) Optimized configuration of different steps along the reaction pathway for *cis*-methyl styrene substrate. The MCM-41 channel was removed for clarity. (I) Isolated oxo-Mn-salen; (II) the anchored complex; (III) docked olefin and encounter-complex of catalyst and substrate; (IV) radical intermediate complex of catalyst and substrate; (V) intermediate state; (VI) complex of reacted catalyst and product; (VII) de-oxygenated anchored catalyst; (VIII) isolated de-oxygenated catalyst. (b) CCM of Mn-salen along the reaction pathway for *cis*- and *trans*-methyl styrene substrates.

alyst (VII), and isolated deoxygenated catalyst (VIII). Fig. 3b shows the CCM of the Mn-salen complex along the reaction pathway for *cis*- and *trans*-substrate as illustrated in Fig. 3a. A transition from cup-like to step-like behavior is evident. This transition provides an explanation for the effectiveness and importance of additional ligand as the immobilizing linker. Our recent DFT geometry optimizations, along with those of Cavallo and Jacobsen [11], show that a homogeneous transition state complex similar to that of V and with chloride as the axial ligand is the most stable species (106 kJ/mol lower than III) within the reaction pathway. In the intermediate state, the olefin strongly interacts with the oxo-Mn center at a specific high chiral configuration of the complex. Although this finding, along with Fig. 3b, suggest that *trans*-olefin has a high level of asymmetric induction to the catalyst, it does not trivially lead to a high ee and catalytic yield. Recent experiments [8] confirmed that when *cis*- is used as the reactant, there is high production of *trans*-epoxide isomer for the immobilized system compared with the *cis*-epoxide. This suggests that in the radical intermediate III, the *trans*-configuration is more favorable because of the less steric hindrances. When the formation of this radical intermediate is the rate-determining step, the influence of *cis*- or *trans*-substrate on enantioselectivity is less pronounced. Understanding the direct effects of substrate on enantioselectivity requires a detailed DFT-based investigation of electronic and steric communication between stereoisomers (substrate or products) and Mn-salen complex. Such studies are beyond the scope of the present work, however. Because of mass transfer limitations, the catalytic activity of Mn-salen complex is often lower than that of homogeneous Mn-salen catalyst [1,6]. During the reaction, Mn-salen complex may selectively bind a (stereo)isomer of the products. The more strongly binding

component will have the lower diffusion rate, giving a bias to the enantiomeric product generated with the lower probability. Moreover, a strong interaction will give maximum chiral selectivity of the more strongly interacting component because of the lower transition state free energy [1,6,11]. The lower diffusivity, originating from nanoporous confinement, can improve chiral recognition (i.e., chirality) and asymmetric induction to the catalyst [8]. The collapse of radical intermediate IV originates a selectivity route that competes with the route based on the product desorptions. Thus, in the overall catalytic process, the enatioselectivity results from two conflicting elementary processes that have opposite effects on the ee. This finding may provide a general reason for the often-observed difference in performance between homogeneous catalysts and their corresponding immobilized catalysts.

## 4. Conclusion

The results presented herein provide new insights into the important steric effects related to linker choices and the interplay with the mesopore channel for anchored oxo-MnV-salen in MCM-41. MD simulations of an anchored (ACM) and a free Mn-salen complex in an MCM-41 channel (FCM) were performed at 273 K and compared with those of a free complex (FCV) and a free complex attached to the linkage in vacuo (FCL). Each MD simulation provides an averaged structure within which its chirality content is quantitatively evaluated with the Avnir CCM. The main finding is that the immobilized linker improves the chiral recognition of the catalyst due to the increasing chirality content of the Mn-salen complex. A *trans*-olefin indicates a high level of asymmetric induction to the Mn-salen catalyst. This, along with the high stability of the intermediate state V [11,13], suggest that the *trans*-olefin can be strongly adsorbed on the oxo-Mn center. Unwanted diffusion limitation of the product may lead to a low ee and catalytic yield. This type of analysis can be of use in evaluating enantioselectivity as well as in designing heterogeneous nanocomposite enantioselective catalysts.

## Acknowledgments

We gratefully acknowledge funding by the Royal Dutch Academy of Sciences and Chinese Academy of Sciences international collaboration program.

## References

[1] C. Li, Catal. Rev. 46 (2004) 419.
[2] S. Xiang, Y. Zhang, Q. Xin, C. Li, Chem. Commun. (2002) 2696.
[3] H. Zhang, S. Xiang, C. Li, Chem. Commun. (2005) 1209.
[4] P. Piaggio, P. McMorn, C. Langham, D. Bethel, P.C. Bulman-Page, F.E. Hancock, G.J. Hutchings, New J. Chem. (1998) 1167.
[5] P. Piaggio, P. McMorn, D. Murphy, D. Bethel, P.C. Bulman-Page, F.E. Hancock, C. Sly, O.J. Kerton, G.J. Hutchings, J. Chem. Soc. Perkin Trans. 2 (2000) 2008.
[6] A. Corma, Catal. Rev. Sci. Eng. 46 (2004) 369.
[7] E.M. McGarrigle, D.G. Gilheany, Chem. Rev. 105 (2005) 1563.
[8] H. Zhang, Y. Zhang, C. Li, J. Catal. 238 (2006) 369.
[9] T. Linker, Angew. Chem. Int. Ed. 36 (1997) 2060.
[10] H. Jacobsen, L. Cavallo, Chem. Eur. J. 7 (2001) 800.
[11] L. Cavallo, H. Jacobsen, Angew. Chem. Int. Ed. 39 (2000) 589.
[12] I.V. Khavrutskii, D.G. Musaev, K. Morokuma, Inorg. Chem. 42 (2003) 2606.
[13] C. Linde, B. Akermark, P.-O. Norrby, M. Svensson, J. Am. Chem. Soc. 121 (1999) 5083.
[14] L. Cavallo, H. Jacobsen, Inorg. Chem. 43 (2004) 2175.
[15] J. El-Bahraoui, O. Wiest, D. Feichtinger, D.A. Plattner, Angew. Chem. Int. Ed. 40 (2001) 2073.
[16] I. Dominguez, V. Fornes, M.J. Sabater, J. Catal. 228 (2004) 92.
[17] V. Ayala, A. Corma, M. Iglesias, F. Sanchez, J. Mol. Catal. 221 (2004) 201.
[18] M.J. Frisch, G.W. Trucks, H.B. Schlegel, G.E. Scuseria, M.A. Robb, J.R. Cheeseman, J.A. Montgomery Jr., T. Vreven, K.N. Kudin, J.C. Burant, J.M. Millam, S.S. Iyengar, J. Tomasi, V. Barone, B. Mennucci, M. Cossi, G. Scalmani, N. Rega, G.A. Petersson, H. Nakatsuji, M. Hada, M. Ehara, K. Toyota, R. Fukuda, J. Hasegawa, M. Ishida, T. Nakajima, Y. Honda, O. Kitao, H. Nakai, M. Klene, X. Li, J.E. Knox, H.P. Hratchian, J.B. Cross, V. Bakken, C. Adamo, J. Jaramillo, R. Gomperts, R.E. Stratmann, O. Yazyev, A.J. Austin, R. Cammi, C. Pomelli, J.W. Ochterski, P.Y. Ayala, K. Morokuma, G.A. Voth, P. Salvador, J.J. Dannenberg, V.G. Zakrzewski, S. Dapprich, A.D. Daniels, M.C. Strain, O. Farkas, D.K. Malick, A.D. Rabuck, K. Raghavachari, J.B. Foresman, J.V. Ortiz, Q. Cui, A.G. Baboul, S. Clifford, J. Cioslowski, B.B. Stefanov, G. Liu, A. Liashenko, P. Piskorz, I. Komaromi, R.L. Martin, D.J. Fox, T. Keith, M.A. Al-Laham, C.Y. Peng, A. Nanayakkara, M. Challacombe, P.M.W. Gill, B. Johnson, W. Chen, M.W. Wong, C. Gonzalez, J.A. Pople, Gaussian 03, ReVision B01, Gaussian, Inc., Wallingford, CT, 2004.
[19] C. Lee, W. Yang, R.G. Parr, Phys. Rev. B 37 (1988) 785.
[20] A. Schafer, C. Huber, R. Ahlrichs, J. Chem. Phys. 100 (1994) 5829.
[21] B.P. Feuston, J.B. Higgins, J. Phys. Chem. 98 (1994) 4459.
[22] Y. He, N.A. Seaton, Langmuir 19 (2003) 10132.
[23] W.F. van Gunsteren, P. Kruger, S.R. Billeter, A.E. Mark, A.A. Eising, W.R.P. Scott, P.H. Heneberger, I.G. Tironi, The GROMOS96 Manual and User Guide, Biomos and Hochschulverlag AG an der ETH Zürich, Groningen, 1996.
[24] W.F. van Gunsteren, J.C. Berendsen, Angew. Chem. Int. Ed. Engl. 29 (1990) 992.
[25] S. Shi, L. Yan, Y. Yang, J. Fisher-Shaulsky, T. Thacher, J. Comput. Chem. 24 (2003) 1059.
[26] E. Mollmann, P. Tomlinson, W.F. Holderich, J. Mol. Catal. 206 (2003) 253.
[27] S.H. Lee, S.G. Choi, Bull. Korean Chem. Soc. 20 (1999) 285.
[28] S.W. de Leeuw, J.W. Perram, E.R. Smith, Proc. R. Soc. London Ser. A 373 (1980) 27.
[29] E. Lindahl, B. Hess, D. van der Spoel, J. Mol. Mod. 7 (2001) 306.
[30] H.J.C. Berendsen, D. van der Spoel, R. van Drunen, Comput. Phys. Commun. 91 (1995) 43.
[31] W. Humphrey, A. Dalke, K. Schulten, J. Mol. Graphics 14 (1996) 33.
[32] L. Bellarosa, F. Zerbetto, J. Am. Chem. Soc. 125 (2003) 1975.
[33] S. Alvarez, P. Alemany, D. Avnir, Chem. Soc. Rev. 34 (2005) 313.
[34] K. Lipkowitz, S. Schefzick, Chirality 14 (2002) 677.
[35] S. Alvarez, S. Schefzick, K. Lipkowitz, D. Avnir, Chem. Eur. J. 9 (2003) 5832.
[36] K. Lipkowitz, S. Schefzick, Chirality 14 (2002) 677.
[37] H. Zabrodsky, S. Peleg, D. Avnir, J. Am. Chem. Soc. 114 (1992) 7843.
[38] H. Zabrodsky, D. Avnir, J. Am. Chem. Soc. 117 (1995) 462.
[39] G. Brancato, F. Zerbetto, J. Phys. Chem. A 104 (2000) 11439.
[40] J.-W. Handgraaf, J.N.H. Reek, L. Bellarosa, F. Zerbetto, Adv. Synth. Catal. 347 (2005) 792.
[41] L. Cavallo, H. Jacobsen, J. Phys. Chem. 107 (2003) 5466.
[42] J.S. Sears, C.D. Sherill, J. Chem. Phys. 124 (2006) 144314.
[43] K.A. Avery, R. Mann, M. Norton, D.J. Willock, Top. Catal. 25 (2003) 89.
[44] S. Chang, J.M. Galvin, E.N. Jacobsen, J. Am. Chem. Soc. 116 (1994) 6937.